

Isotope effect on the few-femtosecond relaxation dynamics of the ethylene cation

Matteo Lucchini^{1,2*}, Manuel Cardosa-Gutierrez^{3*}, Mario Murari¹, Fabio Frassetto⁴, Luca Poletto⁴, Mauro Nisoli^{1,2}, Francoise Remacle^{3†}

¹Department of Physics, Politecnico di Milano, 20133 Milano, Italy

²Institute for Photonics and Nanotechnologies, IFN-CNR, 20133 Milano, Italy

³Theoretical Physical Chemistry, UR MOLSYS, University of Liège, B4000 Liège, Belgium

⁴Institute for Photonics and Nanotechnologies, IFN-CNR, via Trasea 7, 35131 Padova, Italy

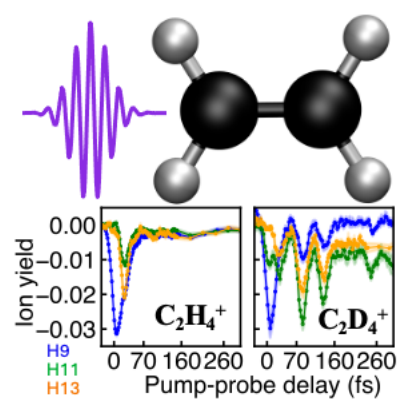
*Equal contribution

Abstract

Few-femtosecond extreme-ultraviolet (EUV) pulses with tunable energy are employed to initiate the Jahn-Teller structural rearrangement in the ethylene cation. We report on a combined experimental and theoretical investigation of an unusual isotope effect on the low energy competing H/D-loss and H₂/D₂-loss channels observed in the ultrafast dynamics induced by an EUV pump pulse and probed by an infrared (IR) pulse. The relative production yield of C₂D₄⁺, C₂D₃⁺, and C₂D₂⁺ exhibit pronounced oscillations with a period of ~50 fs as a function of the pump-probe delay, while the oscillatory patterns are less pronounced for C₂H₄⁺. By using surface hopping to model the non-adiabatic dynamics in the four lowest electronic states of the cation, we show that the enhanced oscillations in deuterated fragment yields arise from a synergy between the isotope effect on the wave packet relaxation through the network of conical intersections and on the vibrational frequencies of the cation.

† Corresponding author: email: fremacle@uliege.be

TOC Graphic



1. Introduction

Recent studies have renewed interest in the ultrafast relaxation and the dynamics of the structural Jahn-Teller rearrangement that follow the sudden ionization of ethylene (C_2H_4) neutral ground state to the lowest electronic states of its cation (C_2H_4^+)¹⁻⁶. This renewed focus is driven by significant advances in generating ultrashort extreme-ultraviolet (EUV) and infrared (IR) pulses, which allow researchers to capture time-resolved electronic and vibronic dynamics with unprecedented detail⁷⁻¹⁰. These ultrashort pulses have enabled direct observation of the intricate molecular motions that occur as the ethylene cation undergoes rapid structural rearrangement, illuminating the crucial roles of conical intersections (CIs) and vibronic couplings in guiding these ultrafast processes. Such insights provide a more detailed understanding of the mechanisms underlying electronic relaxation and molecular reconfiguration on femtosecond time scales. A comprehensive overview of foundational studies in this field can be found in Ref.⁵. The ethylene cation serves as a model system for investigating electronic relaxation pathways, structural dynamics, and energy redistribution after ionization. Dynamics simulations indicate that excited C_2H_4^+ relaxes to the lowest electronic doublet state through CIs, which occurs at both twisted and planar molecular geometries. These CIs facilitate distinct dissociation pathways, leading to H- and H_2 -loss. EUV-pump and IR-probe schemes, which ionize neutral ethylene and then track the ensuing nuclear and electronic dynamics, have confirmed many of these mechanisms experimentally. The high time resolution of these methods has provided critical insights into the relationship between excitation energy, relaxation pathways, and fragment ion yields.

EUV time-resolved photoelectron spectroscopy has further expanded our understanding by examining isotope effects in these ultrafast relaxation dynamics. Experiments using ethylene-d₄ (C_2D_4) reveal notable isotope influences on the time scales and yields of fragmentation processes¹¹. Specifically, deuteration increases the time scale for internal conversion steps by a factor of approximately $\sqrt{2}$, consistent with theoretical predictions that account for the mass-dependent nature of nuclear motion. This delay in dynamics highlights the critical impact of isotopic substitution on the molecular relaxation pathways of ethylene cations.

In this work, we provide evidence for an unexpected isotope effect on charged fragmentation yields, utilizing an advanced few-femtosecond EUV-pump/IR-probe experimental setup. Our results reveal new details on the time-dependent fragmentation pathways in ethylene cation photochemistry, demonstrating that isotope substitution can

significantly modulate ions yields on femtosecond time scales. This study contributes to a deeper understanding of the molecular-level mechanisms driving photochemical reactions in ethylene cations, with broader implications for interpreting isotope effects in other systems undergoing ultrafast nonadiabatic dynamics.

2. Ion yields and population dynamics of the lowest states of the ethylene cation

Briefly, the ethylene neutral ground state (GS) is ionized to the four lowest electronic states of the cation, D_0 , D_1 , D_2 and D_3 , using ~ 10 -fs EUV pulses produced by high-order harmonic generation (HHG) in a gas cell, driven by ~ 15 -fs IR pulses with a central wavelength of about 800 nm. The low order harmonics (9th, 11th and 13th, hereafter indicated as H9, H11 and H13, respectively) are spectrally selected by employing a time-delay compensated monochromator¹²⁻¹⁴ (see Fig. S1 in the Supporting Information (SI)).

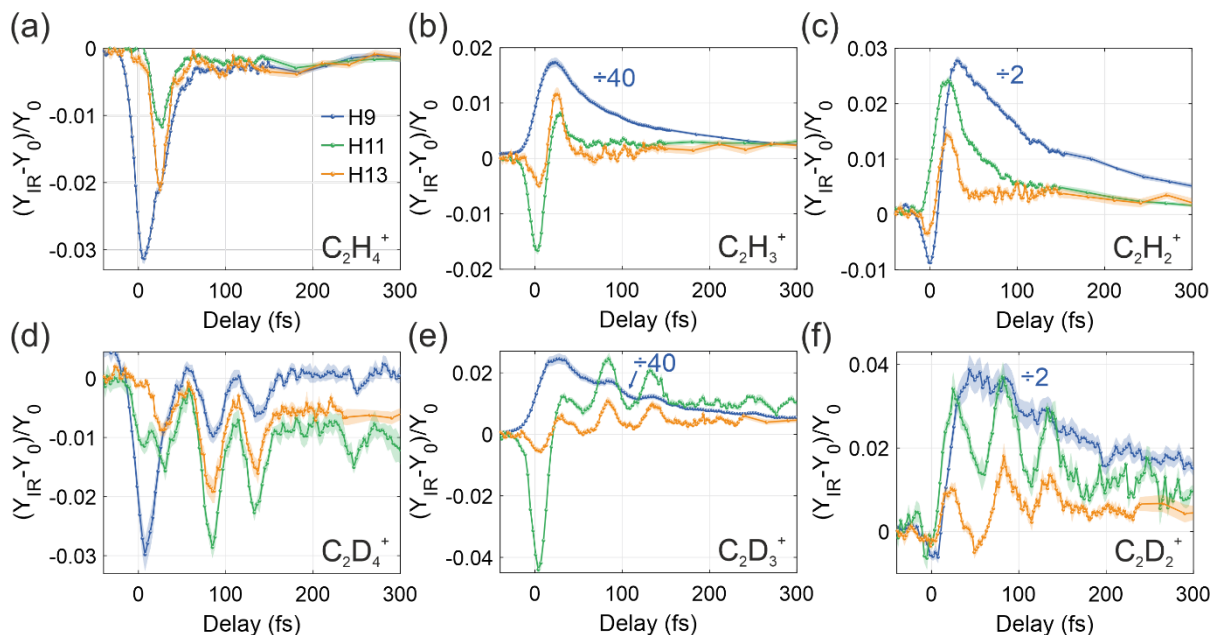


Figure 1: Relative yield as a function of the EUV-IR delay for the fragments (a) $C_2H_4^+$, (b) $C_2H_3^+$, and (c) $C_2H_2^+$, obtained by ionizing ethylene with H9 (blue), H11 (green) and H13 (orange). The second row shows the results in case of ethylene- d_4 ionization: (d) $C_2D_4^+$, (e) $C_2D_3^+$, and (f) $C_2D_2^+$. In all panels, the markers represent the average over 10 independent pump-probe measurements, while the shaded areas cover twice their standard deviation (error of the mean).

Figure 1 shows the differential ion yield, defined as the difference between the ion yield measured with and without the IR pulse, divided by the latter, for the first three heaviest fragments of ethylene (figs. 1(a)-(c)) and ethylene- d_4 (Figs. 1(d)-(f)). The deuterated fragments qualitatively agree with their related hydrogenated counterpart, besides clear amplitude oscillations with a period of ~ 50 fs. Photoionization by H9 leaves the molecule mostly on the GS of the cation, D_0 , with a smaller fraction on the first excited state, D_1 (see Table 1). The

photoionization cross-sections are taken to be identical for the two isotopomers and were derived from the experimental data of Ref.¹⁵ and are in good agreement with computed photoionization cross-sections, see for example ref.¹⁶. The interaction with the IR pulse induces a bleaching of the parent ion, occurring near delay zero (i.e., when pump and probe pulses temporally overlap) for both isotopomers (compare the blue curves in Figs. 1(a) and 1(d)).

Table 1. Relative photoionization yields to the D_0 , D_1 and D_2/D_3 states of the ethylene cation derived from the experimental photoionization cross section reported in Ref. ¹⁵ and the harmonic spectra used in this work. For H13, the ionization yields of higher excited states are $\leq 1\%$ and have been neglected, see SI, section S1.

C₂H₄/C₂D₄	H9	H11	H13
D ₀	0.64	0.23	0.11
D ₁	0.35	0.52	0.28
D ₂ /D ₃	0.01	0.25	0.61

After excitation by H11 (green curves in Fig. 1) and H13 (orange curves in Fig. 1) the cation is left in a higher excited state (see Table 1) and the bleaching occurs at ~ 25 -fs delay time, where a shoulder is observed in $C_2H_4^+$ relative yield from H9 (Fig. 1(a), blue curve). In our previous study³ we have used dynamical surface hopping (SH) for ensembles of trajectories initially started on the ground cationic state and the first three excited states, followed by Born Oppenheimer Molecular Dynamics (BOMD) simulations once the population of the excited cationic states relaxed back to D_0 . We showed that the bleaching peak in the $C_2H_4^+$ yield is due to a re-excitation to D_3 of the population that relaxed to D_0 from higher states or that was ionized to D_0 by the IR probing pulse through a multiphoton process³ (see Fig. 2(a) for a cartoon of the relaxation paths). Re-excitation is favored when a notable fraction of the trajectories on D_0 adopt a geometry that corresponds to a large transition dipole and is three-photon resonant with D_3 . The bleaching peak for H11 and H13 ionization is delayed relative to that for H9 ionization due to the ~ 20 fs needed for the population in the D_1 , D_2 , and D_3 states to relax to D_0 , establishing favorable conditions for re-excitation.

The same mechanism is responsible for the delayed shoulder observed in Fig. 1(a), which is attributed to the re-excitation to D_3 of the population initially excited to D_1 by H9 and that later relaxes to D_0 .³ The short computed lifetime for D_1 (~ 12 fs, see Table S2) in $C_2H_4^+$ supports this argument and is in agreement with similar semiclassical studies.¹⁻⁵ The shoulder is almost absent for the $C_2D_4^+$ H9 yield (Fig. 1(d), blue curve) because of the mass effect on the rate of motion of the wave packet on D_1 for the heavier isotopomer which leads to a longer

computed relaxation lifetime of 26 fs (Table S2) for the D_1 state of $C_2D_4^+$. For the H11 and H13 ionizations of C_2D_4 (green and orange curves in Fig. 1(d)), the delay of the bleaching is comparable to what observed in C_2H_4 . SH non-adiabatic modeling of the population dynamics (see SI, section S2), shows that the different relaxations paths through the network of CI's from the excited states to the GS D_0 are followed in different proportions by the two isotopomers. This is qualitatively sketched by the thickness of the red ($C_2H_4^+$) and blue ($C_2D_4^+$) arrows in the cartoon of Fig. 2(a). Figures 2(b)-(g) show the calculated temporal evolution of the electronic state populations following initial excitation to D_1 (Figs. 2(b) and (e)), D_2 (Figs. 2(c) and (f)) and D_3 (Figs. 2(d) and (g)). The mass isotope effect slows the motion of $C_2D_4^+$ and delays the relaxation from D_1 to D_0 , as shown in the computed decay curve for the D_1 ensemble (compare Figs. 2(b) and (e)). In contrast, there is only a small delay in the relaxation of the D_2 and D_3 ensembles (see Figs. 2(c)-(d) and compare with Figs. 2(f)-(g), respectively) resulting in similar computed lifetimes of these two higher excited states (see Table S2).

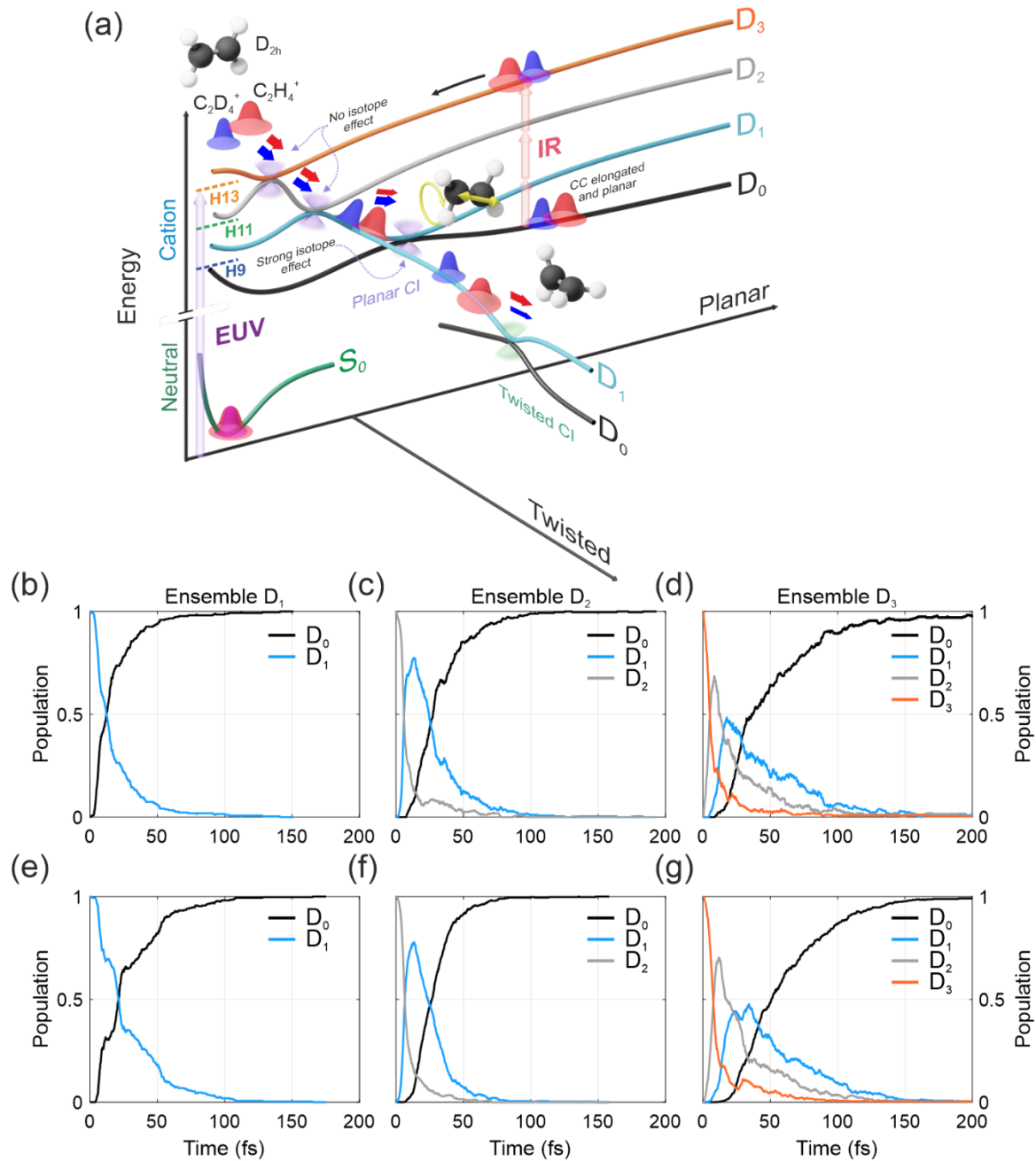


Figure 2: (a) Cartoon of the relaxation paths through the network of CIs between the 4 lowest electronic states, D_0 (black), D_1 (light blue), D_2 (grey) and D_3 (orange), of the ethylene cation for $C_2H_4^+$ (red wavepacket) and $C_2D_4^+$ (blue wavepacket). Also shown is the ground electronic state, S_0 green curve, of the neutral which is suddenly ionized by the EUV pulse (violet arrow on the left). The thickness of the red and blue arrows indicates the difference in the fraction of trajectories that follows a given pathway. The relaxation pathway of the two isotopomers differs on D_1 , where a larger fraction of the heavier $C_2D_4^+$ relaxes to D_0 through the planar I CI (violet cone) than for $C_2H_4^+$, see Table 2. The green cone indicates the twisted CI between D_1 and D_0 . Molecular geometries are given after excitation (D_{2h}) or at the highlighted D_0/D_1 CIs. For the case of the planar I CI, the yellow arrows indicate the torsional motion and CC stretching that are activated at the CI geometry. Finally, the red vertical arrows on the left picture the 3-photon re-excitation process discussed in Ref. ³. Note that the total energy is conserved for each ionization energy meaning that the population on D_0 is vibrationally more excited for H11 and H13 than for H9. (b)-(d), Population dynamics for the hydrogenated molecule corresponding to initial excitation to D_1 , D_2 and D_3 . (e)-(g) same as (b)-(d) but for the deuterated molecule.

3. Isotope effect on the dynamics of the fragmentation yields

Beyond the isotope effect on the timing of the bleaching peak of the parent and the correlated first maximum in the other fragments in Fig. 1, there is a pronounced isotope effect

on the dynamics of the fragmentation yields. The temporal evolution of the relative ion yield of the deuterated species (displayed in Figs. 1(d)-(f)) shows large oscillations with a period of ~ 50 fs (with peaks at ~ 85 fs and ~ 135 fs). In contrast, in the ion yields of the hydrogenated species (Figs. 1(a)-(c)) the oscillations are much weaker, and visible only in the parent ion, with a comparable ~ 50 -fs period. In C_2D_4^+ the oscillations dephase after ~ 150 fs and exhibit a revival after ~ 250 fs for the H11 and H13 ionization (see Fig. S7). A previous experimental-theoretical study of the isotope effect on the fragmentation of the ethylene cation using a higher energy EUV attosecond pulse train and a longer IR pulse probe⁶, focused on monitoring the yields in higher energy fragments (H^+/D^+ , $\text{CH}_2^+/\text{CD}_2^+$). Faster dynamics was reported for C_2H_4^+ , but no oscillations were resolved in the fragmentation yields.

In this Paper, we demonstrate that the large oscillations in the fragment yields in the case of ethylene-d₄ originate from the synergy between two isotope effects on the dynamics, which affect the fraction of the photoionized population that is present or has relaxed to D_0 from the higher excited states and is available for re-excitation by the IR pulse. The first isotope effect is the slowdown of the motion of the wave packets of the deuterated species due to the mass effect, which alters the relaxation paths through the network of the CIs between the electronic states of the cation (see Fig. 2(a)). The second effect involves the mass-dependent changes in the vibrational frequencies of the D_0 state which leads to stronger coupling between the CC stretching and the torsion and scissoring modes in the vibrationally excited C_2D_4^+ cation that control the magnitude of the transition dipole from D_0 to D_3 .

Upon sudden ionization of the neutral ground electronic state in its equilibrium geometry, the ethylene cation is produced in an unstable planar D_{2h} geometry which initiates nuclear motion on the four lowest excited electronic states of the cation, D_0 , D_1 , D_2 and D_3 , that are populated by EUV photoionization in this study (see Fig. 2(a)). The nuclear motion in the excited states triggers ultrafast electronic relaxation in ~ 50 fs through a network of planar and twisted CIs, which leads to fragmentations and isomerizations on the ground electronic state D_0 . Several theoretical studies^{1-6, 17-21} have already identified the essential of the excited state dynamics for the four lowest states of the cation. The CIs seams between the excited states act like geometrical funnels that constrain the geometry of the cation when it relaxes from a higher excited state to a lower one, thereby activating specific nuclear motions. The CIs sampled by the SH trajectories at the level of electronic structure that we use agree with recent previous works^{1, 5}. We provide the geometries of the minimum energy CIs (MECIs) in Section S4.1 of the SI.

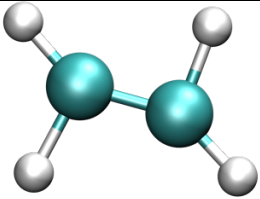
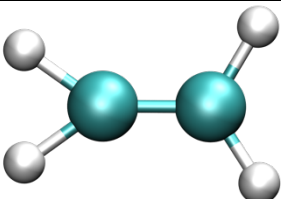
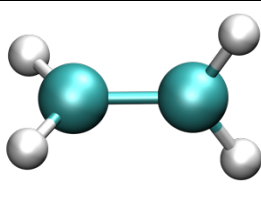
The D_2/D_3 and D_2/D_1 relaxations occur through the seams of two peaked MECIs with planar geometries and elongated C-C bonds ($\sim 1.4\text{\AA}$) (marked with violet cones in Fig. 2(a), see Section S4.1 of the SI). These geometries are close to the planar geometry of the neutral GS of the Franck-Condon (FC) region, which explains why the relaxation is ultrafast and not subject to isotope effect. The D_3/D_2 transfer occurs within 5 fs for both isotopomers (Figs. 2(d) and 2(g)). The population transfer from D_2 to D_1 , instead, happens within 5 to 10 fs for both the D_2 (Figs. 2(c) and 2(f)), and the D_3 (Figs. 2(d) and 2(g)) initial states. In this latter case we observe an additional shoulder at about 15 fs. The D_3/D_2 and D_2/D_1 MECIs activate the C-C elongation and in plane C-H modes. As a result, the populations that reach D_1 within the first 10 fs from D_2 and D_3 exhibit planar geometries which are significantly different from the D_1 ensemble of initial conditions sampled from the Wigner distribution of the D_{2h} planar neutral (see Fig. S9).

Three CIs are involved in the D_1/D_0 relaxation sampled by the SH trajectories: two planar and a twisted one. The two planar CIs were identified in Refs.^{1,5}. We call them planar I and II, respectively. The planar I MECI (violet cones in Fig. 2(a) between D_1 and D_0) is located 2.45 eV above the energy of the planar, D_{2h} , D_0 cation (see Table S3). It has a distorted geometry with modified HCH angles and a slightly compressed C-C bond (1.28 Å). It plays a major role relaxation channel to D_0 for both isotopomers (see Table 2). The second MECI, planar II (not shown in Fig. 2(a)), is slightly higher in energy (2.56 eV, Table S3) and is less sampled in relaxation dynamics of the two isotopomers. Both MECI geometries have a compressed C-C bond. They activate the C-C elongation and CH modes as the D_3/D_2 and D_2/D_1 ones, but to a lesser extent, see Fig. S9, and low frequency, out-of-plane motions: the CH_2 torsion, wagging, and HCH in plane scissoring modes (see SI Section S4.1). The planar MECI geometries (see the molecular cartoon in Fig. 2(a) for planar I) differ more from the planar geometry of the neutral ground state than the D_3/D_2 and the D_2/D_1 MECIs. As a result, the decay of the D_1 initial state to D_0 in Figs. 2(b) and (e) is slower than that of the D_2 and D_3 ones to D_1 , see Figs. 2(c)-(f). The seams of the planar CI's are very shallow. In addition, Frans  n et al.⁵ identified a third planar D_1/D_0 MECI that was not characterized at our level of electronic structure, and that is similar to the one reported in Ref.⁴, see SI section S4.1.

The third major MECI playing a role in the D_1/D_0 relaxation dynamics for the energy range of the three ionization energies discussed here has a twisted MECI geometry with a torsion angle of 90° as previously reported (marked with green cones in Fig. 2(a)).^{1,5,17,18} This CI is lower in energy than the two planar MECI (1.57 eV above the planar D_{2h} geometry of D_0 , Table S3) and activates the out-of-plane low frequency mode CH_2 torsion, wagging, and in plane HCH anti-symmetric bending scissoring, as well as the C-H stretching. Unlike the other

two planar CIs, the C-C stretching is not activated in the twisted CI. We identified a second non-planar MECI of an approximate C_{3v} ethylidene geometry that is however not sampled by the SH trajectories in the first 200 fs, see section S4.1. On the other hand, ethylene/ethylidene isomerization occurs extensively on D_0 for the D_1 , D_2 and D_3 initial states during the 2 ps BOMD dynamics for both isotopomers. It does not however correlate with H_2 loss as speculated in Refs.^{17, 18} and reported by Frans  n et al. for $\sim 2\%$ of trajectories initiated on D_2 and D_3 in the first 200 fs of SH simulations for $C_2H_4^+$, see SI Section S5.

Table 2. Fraction of trajectories that reach D_0 through a hop from D_1 via the three D_1/D_0 CIs (see Fig. S2 for the distribution in time of the last D_1/D_0 hop for the three ensembles of initial conditions on D_1 , D_2 and D_3 respectively). The confidence intervals are reported in Section S4.2.

			
Hydrogen	Planar Type I	Planar Type II	Twisted
Deuterium	52.3	6.4	41.3
	58.7	4.2	37.1
Ensemble D2	81.5	9.4	9.1
	96.3	3.1	0.6
Ensemble D1	77.5	21.1	1.4
	86.4	13.3	0.3

The major channel for the D_1/D_0 relaxation is the planar I CI for the D_1 and the D_2 initial states for both isotopomers, see Table 2. The confidence intervals were assigned using a bootstrapping procedure reported in Section 4.2. Because of the mass effect, the motion of the $C_2D_4^+$ trajectories initiated in the FC region is slowed down compared $C_2H_4^+$. As a result, $C_2D_4^+$ more efficiently relaxes through the planar I CI, which is sloped and close to the FC region in configuration space. For the D_1 ensemble, the isotope mass effect leads to a longer relaxation time, 21.4 fs for $C_2D_4^+$ vs 12.3 fs for $C_2H_4^+$ (see Table S2). The amount of relaxation of the D_1 ensemble through the twisted CI is negligible, $\sim 1\%$ for $C_2H_4^+$ and less than 1% for $C_2D_4^+$. For the D_2 ensemble, for $C_2H_4^+$ the fraction that relaxes through the twisted D_1/D_0 CI reaches 9% and is comparable to the fraction going through the planar II D_1/D_0 CI, while for $C_2D_4^+$ because of the isotope mass effect, these fractions reduce to 3.1 and 0.6% respectively. In the deuterated molecules, this makes the planar I CI the overwhelming channel ($>95\%$) for relaxation for the D_2 ensemble. For the D_3 ensemble, we observe a significant rise in the fraction of trajectories that relax through the twisted D_1/D_0 CI for both isotopomers ($\sim 40\%$). Nevertheless, relaxation

through the planar I CI remains dominant ($\sim 59\%$ for C_2D_4^+ and $\sim 52\%$ C_2D_4^+). For C_2H_4^+ , the D_1/D_0 relaxation pathways identified in this work are in semi-quantitative agreement with those reported in Ref. ⁵, showing an increase in the importance of the twisted one for the D_2 and D_3 initial states. The major differences are that in our computations the twisted pathway is already playing a role for the D_2 initial state and the contribution of a third planar MECI to the D_1/D_0 relaxation in Ref. ⁵.

Since the total energy is conserved, relaxation from the D_1 , D_2 and D_3 initial states leads to a vibrational excitation of D_0 . Moreover, the geometrical constraints imposed by the relaxation through CIs lead to specific distributions of C-C distances, and HCH and HHHH angles on D_0 for the D_1 , D_2 and D_3 initial states (see Fig. S9), which are in turn different from the Wigner distribution on D_0 . The Wigner distributions of CC distance (Fig. 3(a)) and HCH angles on D_0 are narrower than the distributions resulting from the higher electronic states which are centered on larger mean values. In addition, the distributions of C_2D_4^+ are systematically narrower than those of C_2H_4^+ because the mass isotope effect on the vibrational motion. The major difference however is seen in the torsion mode, whose Wigner distribution for the D_0 ensemble is peaked at $\sim \pm 23^\circ$, the values of the twisting angle in the equilibrium geometry (see left panel of Fig. 3(b)). Instead, the distributions of the torsion angle on D_0 are centered around 0° for the ensembles of trajectories initiated on excited electronic states (see right panel of Fig. 3(b)), as a result of the planarity constraint imposed by the D_1/D_0 type I CI and the D_2/D_3 and D_1/D_2 ones. Note that for the D_1 ensemble the distribution of the CC distance peaks at higher value for the C_2D_4^+ than for C_2H_4^+ .

We now examine the origins of the isotope effect leading to the large amplitude oscillations observed in the experimental relative yields of C_2D_4^+ (Fig. 1(d)), C_2D_3^+ (Fig. 1(e)) and C_2D_2^+ (Fig. 1(f)). As discussed above, the reason for the first bleaching peak in the parent yields, accompanied by a maximum in the yield of the other fragments, is common to both C_2D_4 and C_2H_4 , and due to a 3-photon re-excitation process from D_0 to D_3 initiated by the IR pulse (red arrows in Fig. 2(a)).³ After the first bleaching peak, the presence of the oscillations in the yields with a period of ~ 50 fs in Figs. 1(d), (e) and (f) for the deuterated cations results from two isotope effects that primarily affect the fraction that was ionized to D_1 . This fraction contributes 35% for the H9 ionization, 52% for the H11 and 28% for the H13 one (Table 1).

For the D_1 initial state, the slower motion of the C_2D_4^+ cation due to the mass isotope effect favors the relaxation through the planar I CI. The geometries of the C_2D_4^+ cation on D_0 resulting from short times D_1/D_0 hops (see Fig. S8) are planar and have a C-C bond length elongated to ~ 1.4 to ~ 1.6 Å (see Fig. 3(a)), which favors a large transition dipole from D_0 to

D_3 (see Fig. S10) compared to $C_2H_4^+$. As discussed above, the relaxation of the D_2 and D_3 initial states, which are accessed by the H11 (25%) and H13 (65%) ionizations, leads to wider distributions of the C-C elongation (see Fig. S9) which do not correspond to large values of the D_0/D_3 transition dipole, see Fig. S10 and therefore yield smaller active fractions (Fig. S11).

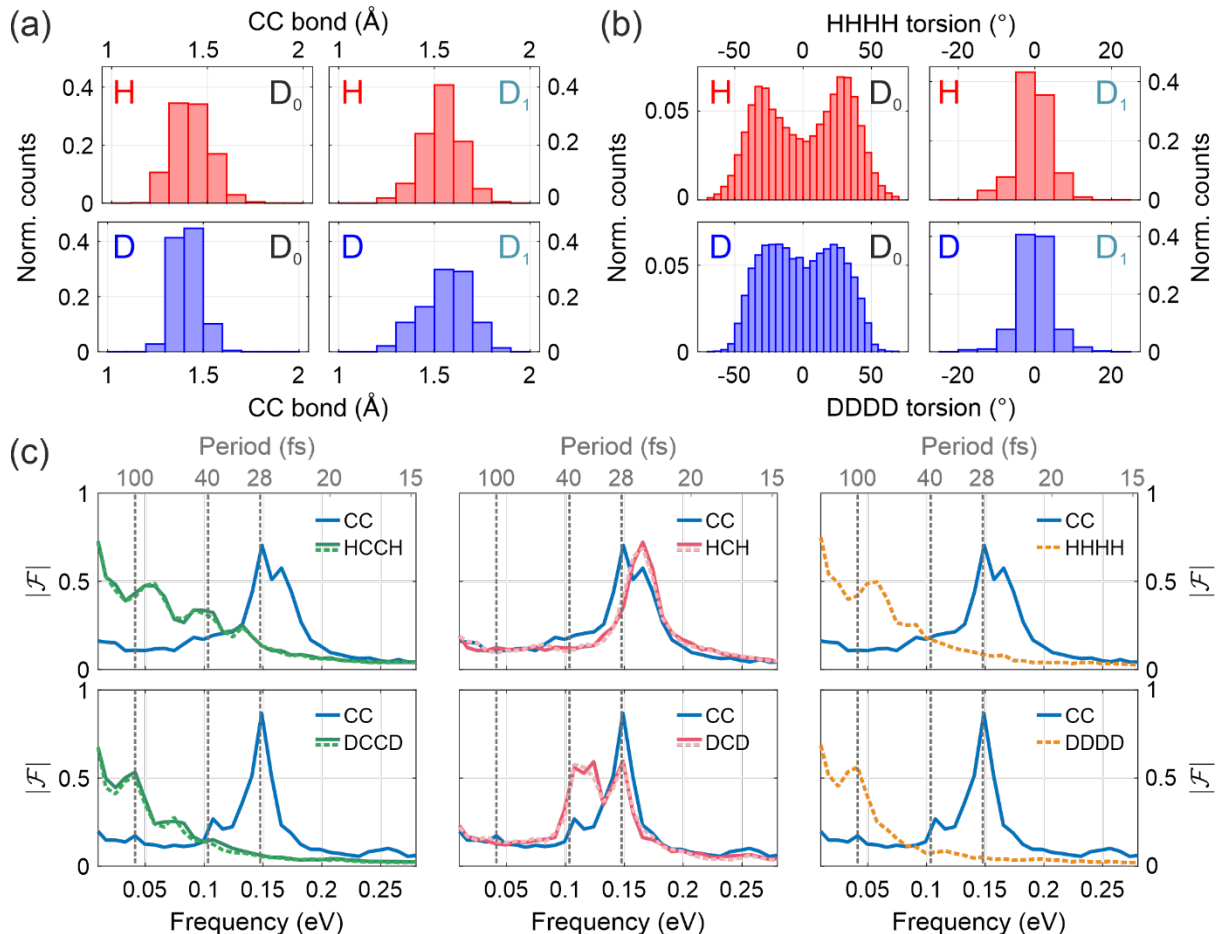


Figure 3: a) Histograms of the C-C bond length for ethylene (red, upper row) and ethylene-d₄ (blue, lower row). The left column shows the results for the Wigner distributions of initial conditions of the D_0 ensemble. The right column shows the distribution after relaxation through the planar I CI in the first 10 fs of the SH dynamics for the D_1 ensemble. b) Same as in a), but for the HHHH (red) and DDDD (blue) angles. Both in a) and b) the number of counts is normalized by the total number of considered trajectories. c) Average Fourier transform of the C-C bond length (blue), HCCH torsion angles (dashed-light and solid-dark green), HCH angles (dashed-light and solid-dark pink), and of HHHH torsion (dashed orange) for $C_2H_4^+$ (top) and $C_2D_4^+$ (bottom) computed for the trajectories of D_1 ensemble that relax on D_0 through the type I CI.

A large value of the transition dipole also requires a bending angle of $\sim 120^\circ$, a condition that is satisfied for both isotopomers (see Fig. S9). The second isotope effect is on the vibrational motions that involve a motion of the D atoms on D_0 . In the case of $C_2D_4^+$, the periods of the C-C elongation and the antisymmetric scissoring DCD modes become almost identical, and in addition also become commensurate with the excited states of torsion mode activated by the relaxation through the planar type I CI or by the ionization process.^{1, 4, 5} The coupling between

these three modes results in combination bands,^{19, 20} which do not occur for $C_2H_4^+$. The periods of the C-C, HCH (DCD), HCCH (DCCD) and HHHH (DDDD) coordinates averaged over the trajectories of the D_1 ensemble that relaxed to D_0 through the planar type I CI are computed by Fourier Transform (FT)²² and plotted in Fig. 3(c) for the two isotopomers. The computed periods are in good agreement with the ones computed at the BOMD level of electronic structure for the equilibrium geometry of D_0 , see Table S7 of the SI. For $C_2D_4^+$, bottom row in Fig. 3(c), the computed periods of the C-C bond and of the antisymmetric scissoring DCD mode appear at ~ 28 fs, the symmetric scissoring DCD mode at ~ 38 fs and the DCCD torsion mode at ~ 100 fs. From the bottom middle panel, one sees that C-C is strongly coupled to the two DCD modes. In addition, the C-C mode exhibits a small peak at 100 fs (marked by a vertical black dashed line in the bottom left and right panels of Fig. 3(c)) which indicates that the C-C mode is coupled to the DCCD torsion. In $C_2H_4^+$ (top row of Fig. 3(c)) the isotope effect on the period of the torsion mode (~ 70 fs) prevents an effective coupling between the torsion and the C-C mode, whose period is unaffected. As a result, as seen from the top left and right panels of Fig. 3(c), there is no peak at 70 fs in the C-C mode. On the other hand, the periods of the two HCH scissoring modes are shifted to shorter values by a factor of ~ 1.3 . The antisymmetric scissoring HCH mode has a period of ~ 21 fs and the symmetric one ~ 29 fs which leads to a strong coupling with the C-C mode. For both isotopomers, the broad peaks in the HCCH coordinate at ~ 45 -50 fs for $C_2H_4^+$ and at ~ 55 -60 fs for $C_2D_4^+$ correspond to the wagging modes.

In $C_2D_4^+$, the computed period of ~ 100 fs for the torsion mode implies that the ion is planar every half period, that is, every ~ 50 fs, which roughly corresponds to two vibrations of the C-C mode. Moreover, for the fraction of trajectories of the D_1 ensemble that relaxes to D_0 through the planar I CI, the C-C bond is elongated. Therefore, for $C_2D_4^+$, a larger transition probability to D_3 occurs each time the C-C is elongated between 1.55 and 1.60 Å, and the cation is planar, see Figure S9, that is, every ~ 50 fs. This correlation is present in 77 trajectories out of the 141 runs for the D_1 ensemble (55 %). The re-excitation to D_3 leads to a bleaching of the parent yield and a simultaneous increase in the fragment yields since fragmentation is favored by the higher excitation energy that is gained through the excitation to D_3 by the 3 IR photon. The computed active fractions on D_0 for the D_2 and D_3 initial states that contribute for 25% for the H11 ionization and 65% for the H13 ionization are significantly smaller, see Figs. S11 of the SI.

Figure 4 shows, as a function of time, the active fraction of trajectories on D_0 that relax from D_1 through the planar CI I with planar geometry (within $\pm 10^\circ$) and with a C-C bond between 1.55 and 1.6 Å, normalized to the D_1 initial state. For $C_2H_4^+$ (shown in Fig. 4(a)), the calculated active fraction shows no clear periodic maxima beyond the bleaching peak at ~ 20 fs. In contrast, $C_2D_4^+$ (shown in Fig. 4(b)) exhibits peaks at around 36 fs, 85 fs and 135 fs, closely matching the timing of the maxima observed in the experimental yields in Figs. 1(d)-(f). The reason for the lack of periodic maxima in $C_2H_4^+$ is the isotope effect on the vibrational frequencies, which precludes an efficient coupling between the CC and the torsion modes. In addition, the shorter vibrational periods of the $C_2H_4^+$ ion induce a faster dephasing between the CC, the torsion modes and the other vibrational modes.

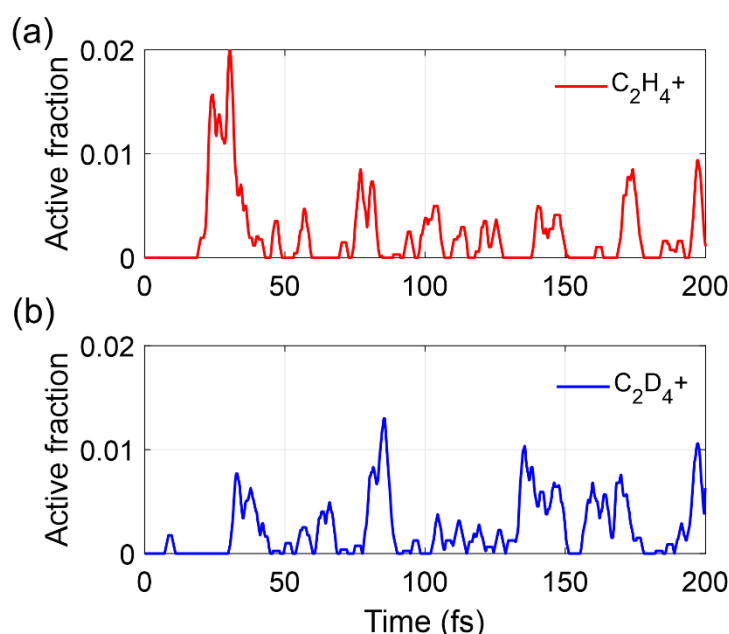


Figure 4: Active fraction of trajectories on D_0 that relax from D_1 through the planar I CI with geometries planar, within $\pm 10^\circ$, and with a CC bond in the range [1.55-1.60] Å) that can be re-excited to D_3 by a three photon transition for $C_2H_4^+$ (red, panel a)) and for $C_2D_4^+$ (blue, panel b)). The continuous thick curves are the result of a mobile average over 25 time points, see SI, Section 4.3 for details on the computation of the active fraction and the computed fractions for the D_2 and D_3 initial states. The computed FTs of the active fraction are reported in Fig. S12. Periods at ~ 50 and ~ 100 fs are resolved for $C_2D_4^+$ while there are not discernable for $C_2H_4^+$.

4. Conclusions and perspectives

In conclusion, by elucidating the enhanced oscillations observed in the relative fragmentation yields of $C_2D_4^+$, our work sheds light on the physical origins of the isotope effect in the ultrafast relaxation process of a prototypical molecular cation. The experimentally measured yields for the deuterated isotopomer exhibit pronounced oscillations with a ~ 50 -fs period which are not clearly discernable for the hydrogenated one. We show that the slower

motion of the wave packet out of the FC region of the heavier C_2D_4^+ for the population ionized to the D_1 electronic state favors the relaxation through the planar type I D_1/D_0 CI. This CI functions as both a geometrical and temporal funnel, transferring a substantial population to D_0 within the initial 10 fs of relaxation with elongated C-C bonds and planar geometries. In addition, in C_2D_4^+ , because of the isotope effect on the vibrational periods, the torsion mode is efficiently coupled to the C-C mode and the cation is planar, with an elongated C-C bond every 50 fs, which corresponds to half the period of the torsion and two periods of the C-C elongation. As a result, the re-excitation to D_3 occurs every 50 fs which explains the larger oscillations in the measured ion yields as a function of the EUV-IR pump-probe delay. The periods of these two modes are not commensurate in C_2H_4^+ which precludes the observation of large oscillations in the ion yields as a function of the EUV-IR pump probe delay.

Our results show that pump-probe schemes based on few-fs tunable EUV radiation in combination with few-fs IR pulses and isotope substitution, provide a fine probe of the geometrical and temporal constraints that the ultrafast relaxation through a network of CIs between excited electronic states imposes on the vibrational motion on the ground electronic state. Our results pave the way for exploiting these constraints for better controlling the reaction outcomes.

Acknowledgments

This project has received funding from the European Research Council (ERC): ERC Synergy grant agreement no. 951224, TOMATTO. FR and MCG acknowledge the support of the Fonds National de la Recherche (F.R.S.-FNRS, Belgium), #T0205.20 and #T.0247.24, and of the action of concerted research MECHANOCHEM (ARC 19/23-20, ULiege). Computational resources have been provided by the Consortium des Equipements de Calcul Intensif (CECI), funded by the F.R.S.-FNRS under Grant # 2.5020.11 The authors thank the COST action ATTOCHEM (CA18222). FR and MC thank Dr. B. Mignolet and Ms Julie Hammoud for useful discussions.

Supporting Information available: Additional information on the experimental set-up, on the electronic structure, SH modeling, MECI's and analysis of the trajectories.

References

- (1) Joalland, B.; Mori, T.; Martínez, T. J.; Suits, A. G. Photochemical Dynamics of Ethylene Cation $C_2H_4^+$. *J. Phys. Chem. Lett.* **2014**, *5* (8), 1467-1471. DOI: 10.1021/jz500352x.
- (2) Ludwig, A.; Liberatore, E.; Herrmann, J.; Kasmi, L.; López-Tarifa, P.; Gallmann, L.; Rothlisberger, U.; Keller, U.; Lucchini, M. Ultrafast Relaxation Dynamics of the Ethylene Cation $C_2H_4^+$. *J. Phys. Chem. Lett.* **2016**, *7* (10), 1901-1906. DOI: 10.1021/acs.jpcclett.6b00646.
- (3) Lucchini, M.; Mignolet, B.; Murari, M.; Gonçalves, C. E. M.; Lucarelli, G. D.; Frassetto, F.; Poletto, L.; Remacle, F.; Nisoli, M. Few-Femtosecond $C_2H_4^+$ Internal Relaxation Dynamics Accessed by Selective Excitation. *J. Phys. Chem. Lett.* **2022**, *13* (48), 11169-11175. DOI: 10.1021/acs.jpcclett.2c02763.
- (4) Zinchenko, K. S.; Ardana-Lamas, F.; Seidu, I.; Neville, S. P.; van der Veen, J.; Lanfaloni, V. U.; Schuurman, M. S.; Wörner, H. J. Sub-7-femtosecond conical-intersection dynamics probed at the carbon K-edge. *Science* **2021**, *371* (6528), 489. DOI: 10.1126/science.abf1656.
- (5) Fransén, L.; Tran, T.; Nandi, S.; Vacher, M. Dissociation and Isomerization Following Ionization of Ethylene: Insights from Nonadiabatic Dynamics Simulations. *J. Phys. Chem. A* **2024**, *128* (8), 1457-1465. DOI: 10.1021/acs.jpca.3c06512.
- (6) Vacher, M.; Boyer, A.; Lorient, V.; Lépine, F.; Nandi, S. Few-Femtosecond Isotope Effect in Polyatomic Molecules Ionized by Extreme Ultraviolet Attosecond Pulse Trains. *J. Phys. Chem. A* **2022**, *126* (34), 5692-5701. DOI: 10.1021/acs.jpca.2c03487.
- (7) Krausz, F.; Ivanov, M. Attosecond physics. *Rev. Mod. Phys.* **2009**, *81* (1), 163-234.
- (8) Nisoli, M.; Decleva, P.; Calegari, F.; Palacios, A.; Martín, F. Attosecond Electron Dynamics in Molecules. *Chem. Rev.* **2017**, *117* (16), 10760-10825. DOI: 10.1021/acs.chemrev.6b00453.
- (9) Borrego-Varillas, R.; Lucchini, M.; Nisoli, M. Attosecond spectroscopy for the investigation of ultrafast dynamics in atomic, molecular and solid-state physics. *Rep. Prog. Phys.* **2022**, *85* (6), 066401. DOI: 10.1088/1361-6633/ac5e7f.
- (10) Merritt, I. C. D.; Jacquemin, D.; Vacher, M. Attosecond Chemistry: Is Controlling Electrons the Future of Photochemistry? *J. Phys. Chem. Lett.* **2021**, *12* (34), 8404-8415. DOI: 10.1021/acs.jpcclett.1c02016.
- (11) Boyer, A.; Humeniuk, A.; Karashima, S.; Suzuki, T. Deuterium Isotope Effect on Internal Conversion of Ethylene Studied by Time-Resolved Photoelectron Spectroscopy. *J. Phys. Chem. A* **2024**, *128* (34), 7068-7072. DOI: 10.1021/acs.jpca.4c02647.
- (12) Lucchini, M.; Lucarelli, G. D.; Murari, M.; Trabattini, A.; Fabris, N.; Frassetto, F.; De Silvestri, S.; Poletto, L.; Nisoli, M. Few-femtosecond extreme-ultraviolet pulses fully reconstructed by a ptychographic technique. *Opt. Express* **2018**, *26* (6), 6771-6784. DOI: 10.1364/OE.26.006771.
- (13) Poletto, L.; Villaresi, P.; Frassetto, F.; Calegari, F.; Ferrari, F.; Lucchini, M.; Sansone, G.; Nisoli, M. Time-delay compensated monochromator for the spectral selection of extreme-ultraviolet high-order laser harmonics. *Rev. Sci. Instrum.* **2009**, *80* (12), 123109. DOI: 10.1063/1.3273964 (accessed 9/13/2024).
- (14) Csizmadia, T.; Filus, Z.; Grósz, T.; Ye, P.; Gulyás Oldal, L.; De Marco, M.; Jójárt, P.; Seres, I.; Bengery, Z.; Gilicze, B.; et al. Spectrally tunable ultrashort monochromatized extreme ultraviolet pulses at 100 kHz. *APL Photonics* **2023**, *8* (5), 056105. DOI: 10.1063/5.0147576 (accessed 9/13/2024).
- (15) Berkowitz, J. "Absolute Partial Cross-Sections of Ethylene (C_2H_4). In *Atomic and Molecular Photoabsorption*, Amsterdam; Elsevier, 2015; pp 442-458.
- (16) Takeshita, K. A theoretical study on ionization of ethylene with analysis of vibrational structure of the photoelectron spectra. *J. Chem. Phys.* **1991**, *95* (3), 1838-1846. DOI: 10.1063/1.461033 (accessed 2/2/2025).

- (17) Lorquet, J. C.; Sannen, C.; Raseev, G. Dissociation of the ethylene cation: mechanism of energy randomization. *J. Am. Chem. Soc.* **1980**, *102* (27), 7976-7977. DOI: 10.1021/ja00547a045.
- (18) Sannen, C.; Raşeev, G.; Galloy, C.; Fauville, G.; Lorquet, J. C. Unimolecular decay paths of electronically excited species. II. The C₂H⁺ ion. *J. Chem. Phys.* **1981**, *74* (4), 2402-2411. DOI: 10.1063/1.441361 (accessed 4/2/2024).
- (19) Pollard, J. E.; Trevor, D. J.; Reutt, J. E.; Lee, Y. T.; Shirley, D. A. Torsional potential and intramolecular dynamics in the C₂H⁺ photoelectron spectra. *J. Chem. Phys.* **1984**, *81* (12), 5302-5309. DOI: 10.1063/1.447672 (accessed 4/2/2024).
- (20) Willitsch, S.; Hollenstein, U.; Merkt, F. Ionization from a double bond: Rovibronic photoionization dynamics of ethylene, large amplitude torsional motion and vibronic coupling in the ground state of C₂H⁺. *J. Chem. Phys.* **2004**, *120* (4), 1761-1774. DOI: 10.1063/1.1635815 (accessed 3/22/2024).
- (21) Wörner, H. J.; Merkt, F. Jahn–Teller Effects in Molecular Cations Studied by Photoelectron Spectroscopy and Group Theory. *Angew. Chem. Int. Ed.* **2009**, *48* (35), 6404-6424, <https://doi.org/10.1002/anie.200900526>. DOI: <https://doi.org/10.1002/anie.200900526> (accessed 2021/09/19).
- (22) Sewell, T. D.; Thompson, D. L.; Levine, R. D. Mode selectivity in the classical power spectra of highly vibrationally excited molecules. *J. Phys. Chem.* **1992**, *96* (20), 8006-8022. DOI: 10.1021/j100199a035.